

Table 3. Properties of FCC 35

Parameter	Value
RA(J2000)	$03^h25^m04^s$
Dec(J2000)	$-36^\circ55'34''.5$
d	18.2 Mpc
$V_{r,\odot}$	1800 km s^{-1}
$\Delta V_{50}(\text{Parkes})$	38 km s^{-1}
$\Delta V_{50}(\text{ATCA})$	50 km s^{-1}
i	62°
$D_{HI}(3 \text{ mJy contour})$	$4'$
M_V	-16.1
E(B-V)	0
M_{tot}	$4.8 \times 10^8 M_\odot$
M_{tot}/L_V	$2.9 M_\odot/L_\odot$
$F_{HI}(\text{ATCA})$	2.9 Jy km s^{-1}
$F_{HI}(\text{Parkes})$	2.8 Jy km s^{-1}
$M_{HI}(\text{ATCA})$	$2.2 \times 10^8 M_\odot$
$M_{HI}(\text{Parkes})$	$2.2 \times 10^8 M_\odot$
$N_{HI(max)}(\text{ATCA})$	$1.1 \times 10^{20} \text{ cm}^{-2}$

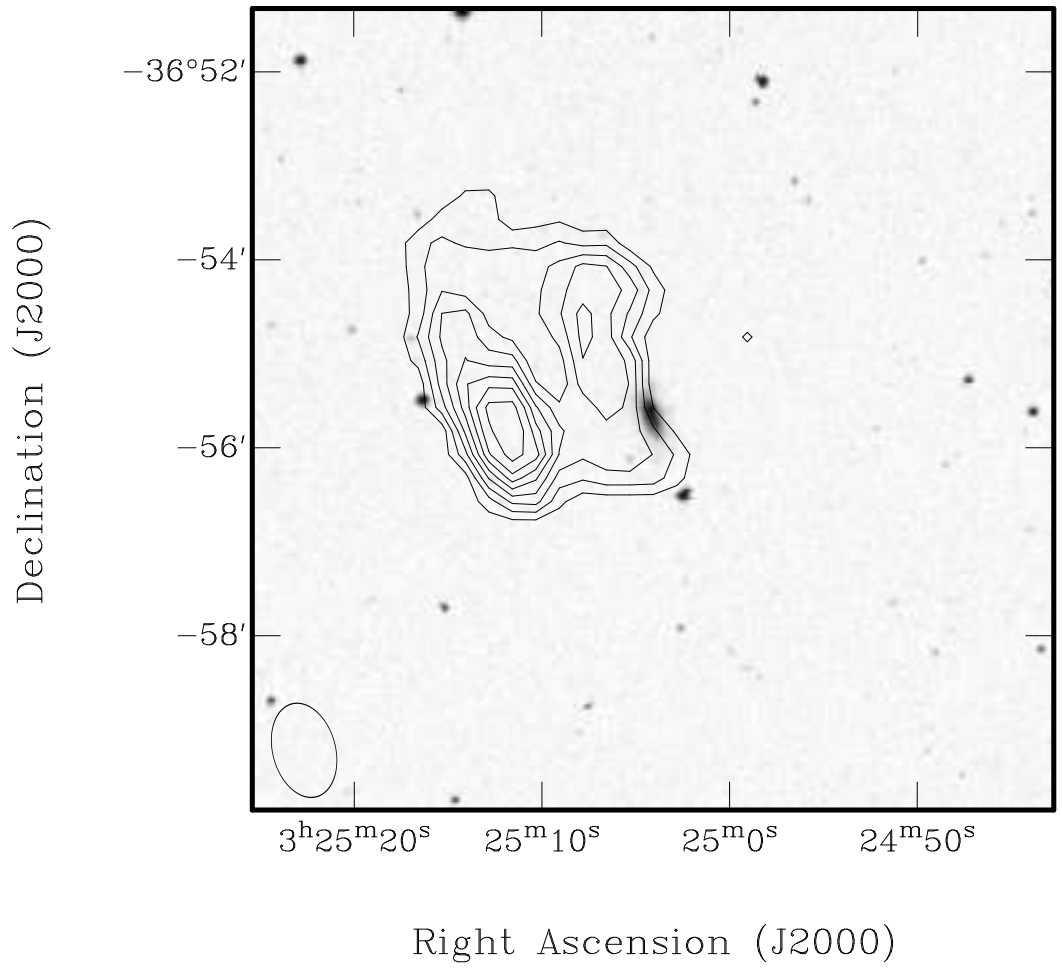


Table 4. Properties of the H I Cloud

Parameter	Value
RA(J2000)	$03^h 25^m 08^s$
Dec(J2000)	$-36^\circ 55' 34''.5$
d	18.2 Mpc
$V_{r,\odot}$	1658 km s^{-1}
$\Delta V_{50}(\text{Parkes})$	52 km s^{-1}
$\Delta V_{50}(\text{ATCA})$	30 km s^{-1}
$D_{HI}(3 \text{ mJy contour})$	$\approx 2' \times 4'$
$F_{HI}(\text{ATCA})$	1.4 Jy km s^{-1}
$F_{HI}(\text{Parkes})$	2.9 Jy km s^{-1}
$M_{HI}(\text{ATCA})$	$1.1 \times 10^8 M_\odot$
$M_{HI}(\text{Parkes})$	$2.2 \times 10^8 M_\odot$
$N_{HI(max)}(\text{ATCA})$	$2.0 \times 10^{19} \text{ cm}^{-2}$

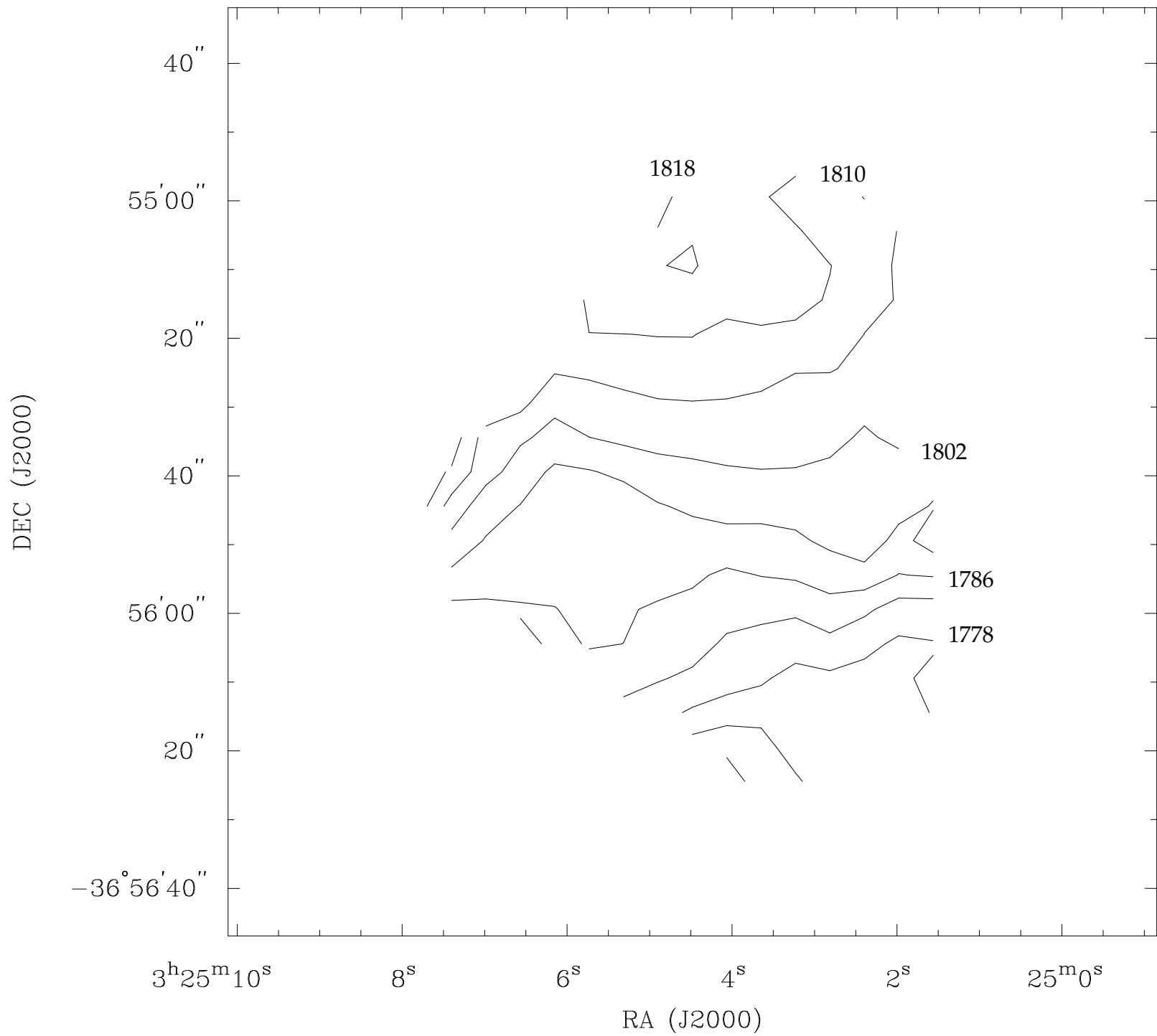


Table 5. Rotation Curve Data

r (")	V_{rot} (km s ⁻¹)	σ_D (km s ⁻¹)	V_c (km s ⁻¹)
6	3.28	3.89	5.09
14	7.80	7.83	11.05
22	12.05	12.67	17.49
30	16.02	18.42	24.41
38	19.21	23.59	30.42
46	20.25	20.79	29.02
54	20.88	8.54	22.56
62	19.71	2.22	19.83

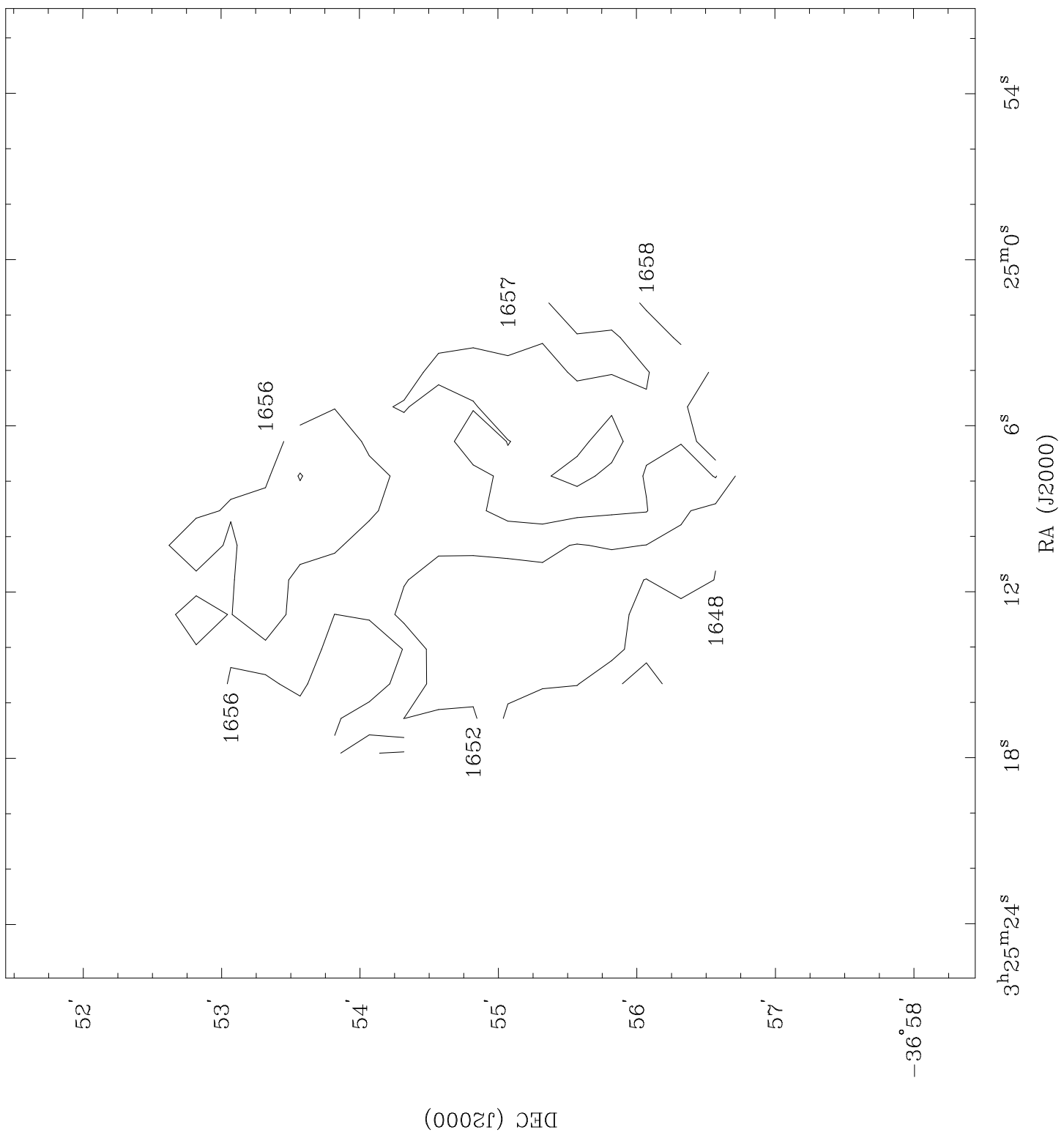


Table 6. Surface Brightness Profiles

R (")	μ_U (mag arcsec ⁻²)	μ_V (mag arcsec ⁻²)	μ_I (mag arcsec ⁻²)
0.60	20.72	21.46	20.89
0.66	20.73	21.54	20.91
0.73	20.74	21.54	20.92
0.80	20.75	21.49	20.92
0.88	20.76	21.44	20.92
0.97	20.78	21.45	20.92
1.06	20.81	21.53	20.91
1.17	20.86	21.61	20.93
1.29	20.89	21.58	20.97
1.41	20.93	21.53	20.97
1.56	20.98	21.52	20.97
1.71	21.02	21.52	20.98
1.88	21.06	21.50	20.98
2.07	21.09	21.25	20.90
2.28	21.13	21.26	20.91
2.51	21.17	21.28	20.93
2.76	21.21	21.29	20.91
3.03	21.25	21.33	20.93
3.34	21.29	21.43	20.97
3.67	21.33	21.46	21.00
4.04	21.32	21.50	21.02
4.44	21.38	21.44	21.00
4.88	21.41	21.39	20.97
5.37	21.52	21.55	21.04
5.91	21.59	21.58	21.06
6.50	21.62	21.68	21.15
7.15	21.69	21.75	21.22

Table 6—Continued

R (")	μ_U (mag arcsec ⁻²)	μ_V (mag arcsec ⁻²)	μ_I (mag arcsec ⁻²)
7.87	21.82	21.85	21.28
8.65	21.98	22.03	21.42
9.52	22.20	22.21	21.55
10.47	22.37	22.36	21.70
11.52	22.58	22.54	21.86
12.67	22.82	22.70	21.98
13.94	22.97	22.85	22.11
15.33	23.45	23.08	22.27
16.86	23.75	23.34	22.55
18.55	24.02	23.58	22.71
20.40	24.34	23.85	23.06
22.44	24.96	24.16	23.35
24.69	25.23	24.87	23.89
27.16	25.67	25.45	24.26

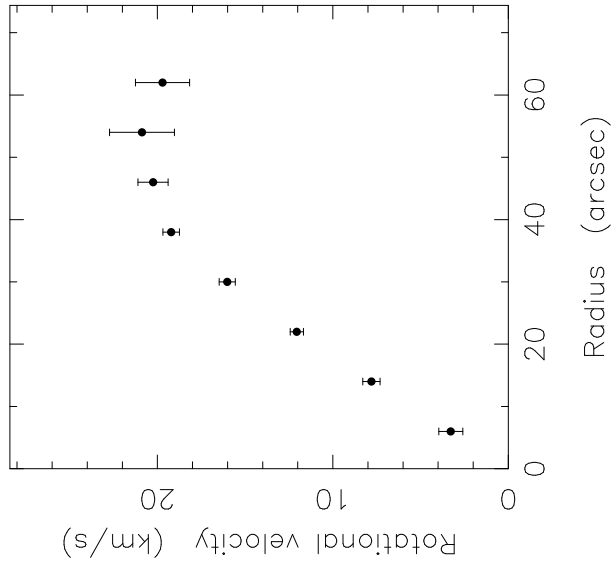
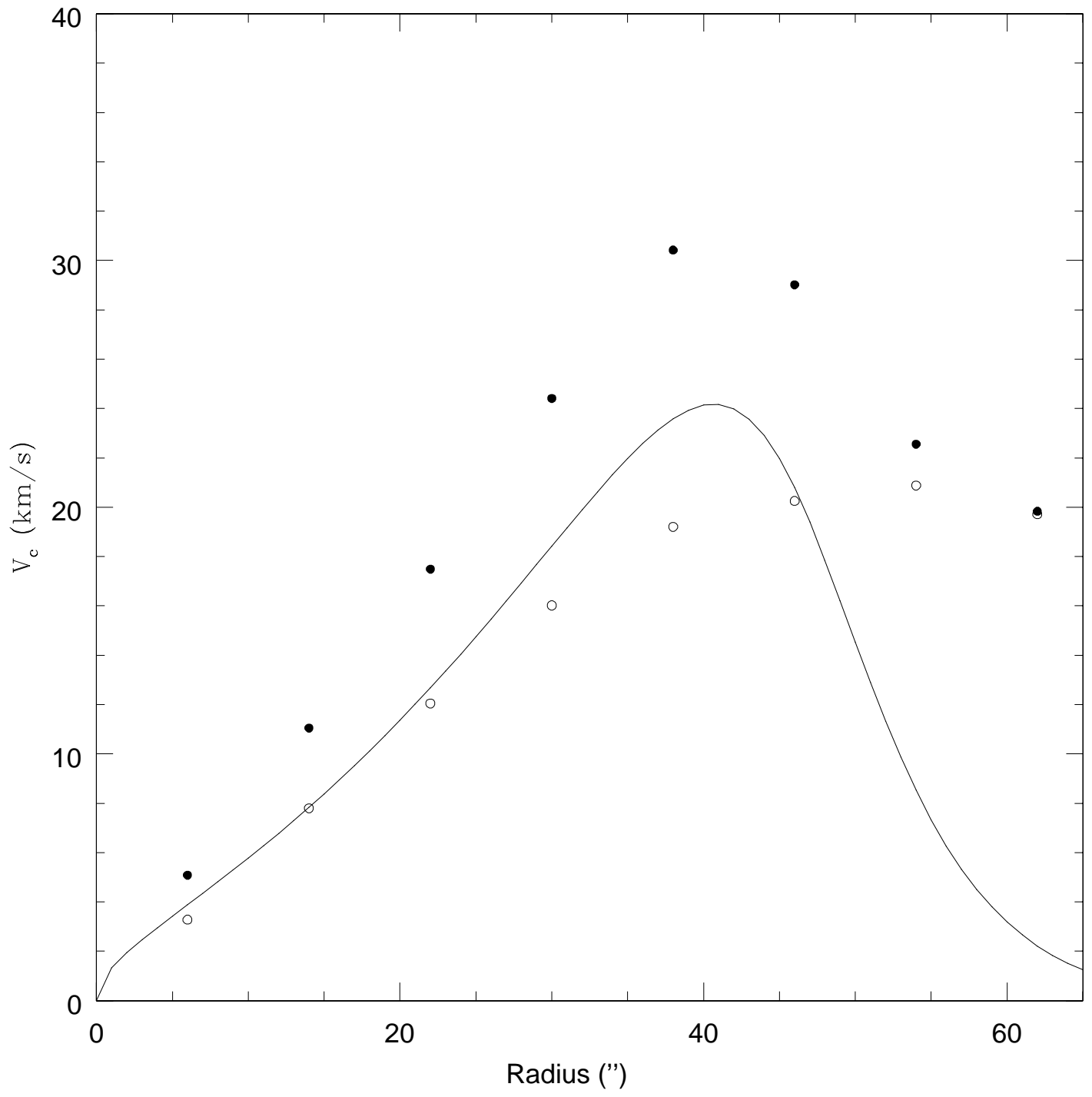
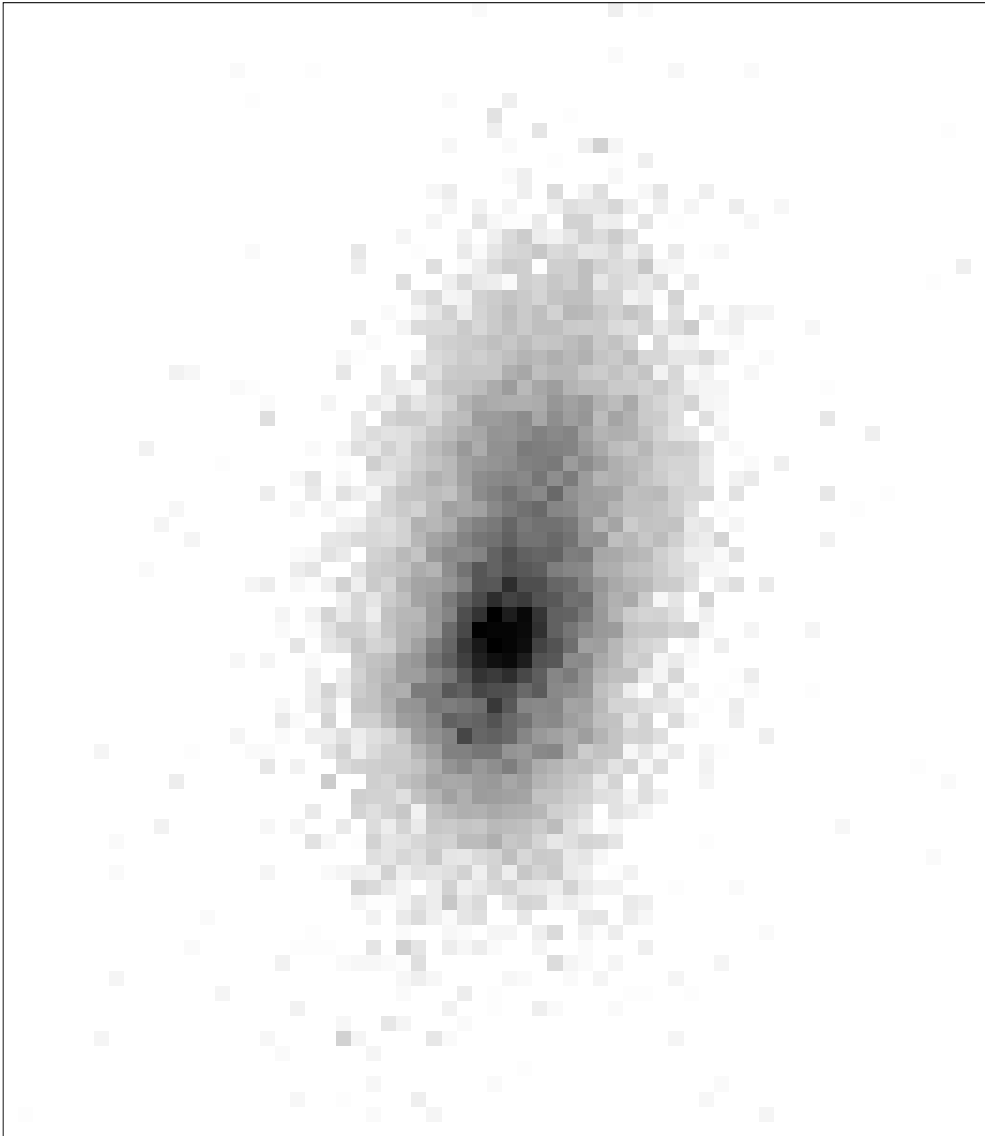


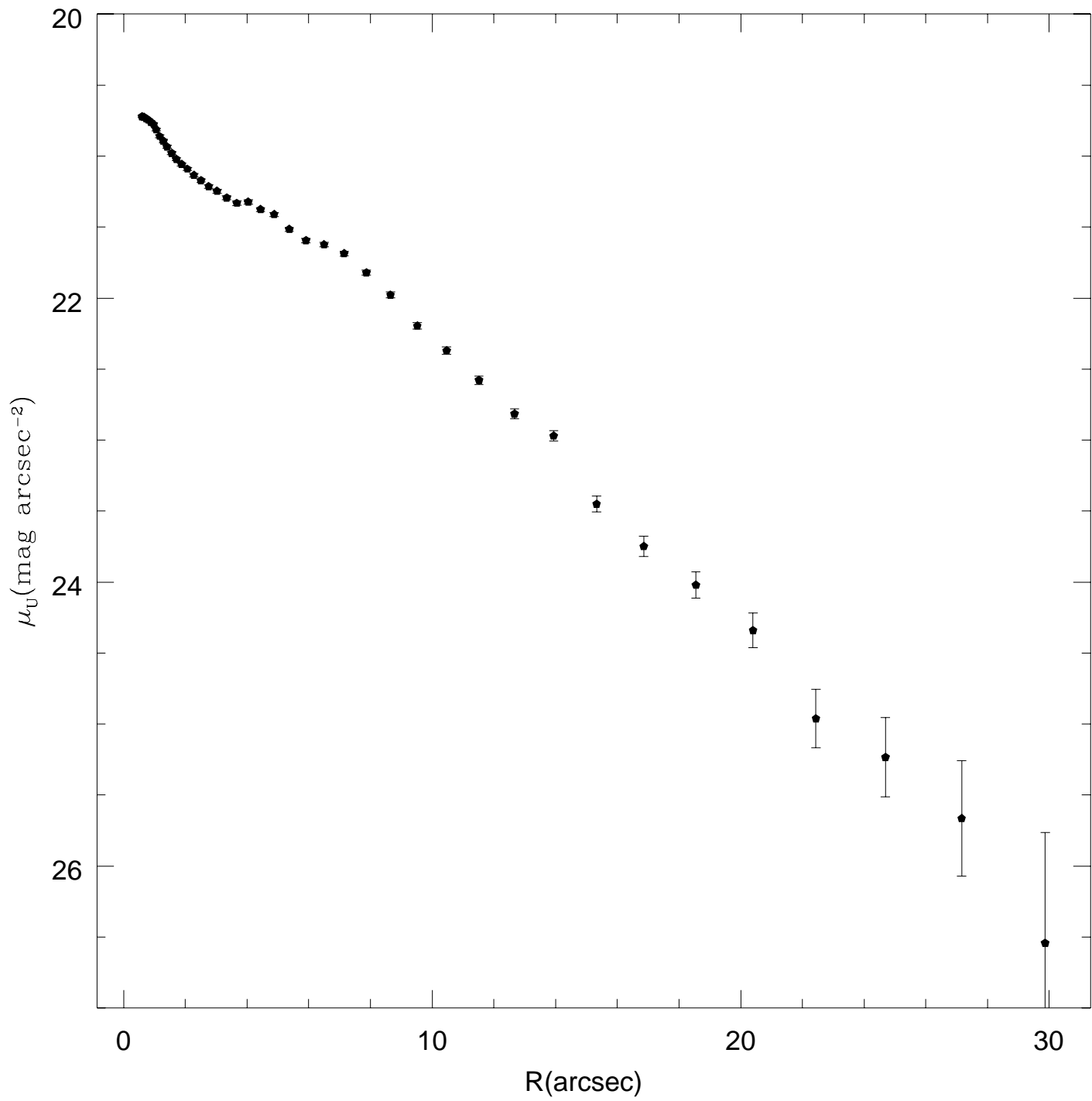
Table 7. Optical Photometry: Circular apertures around the off-center nucleus

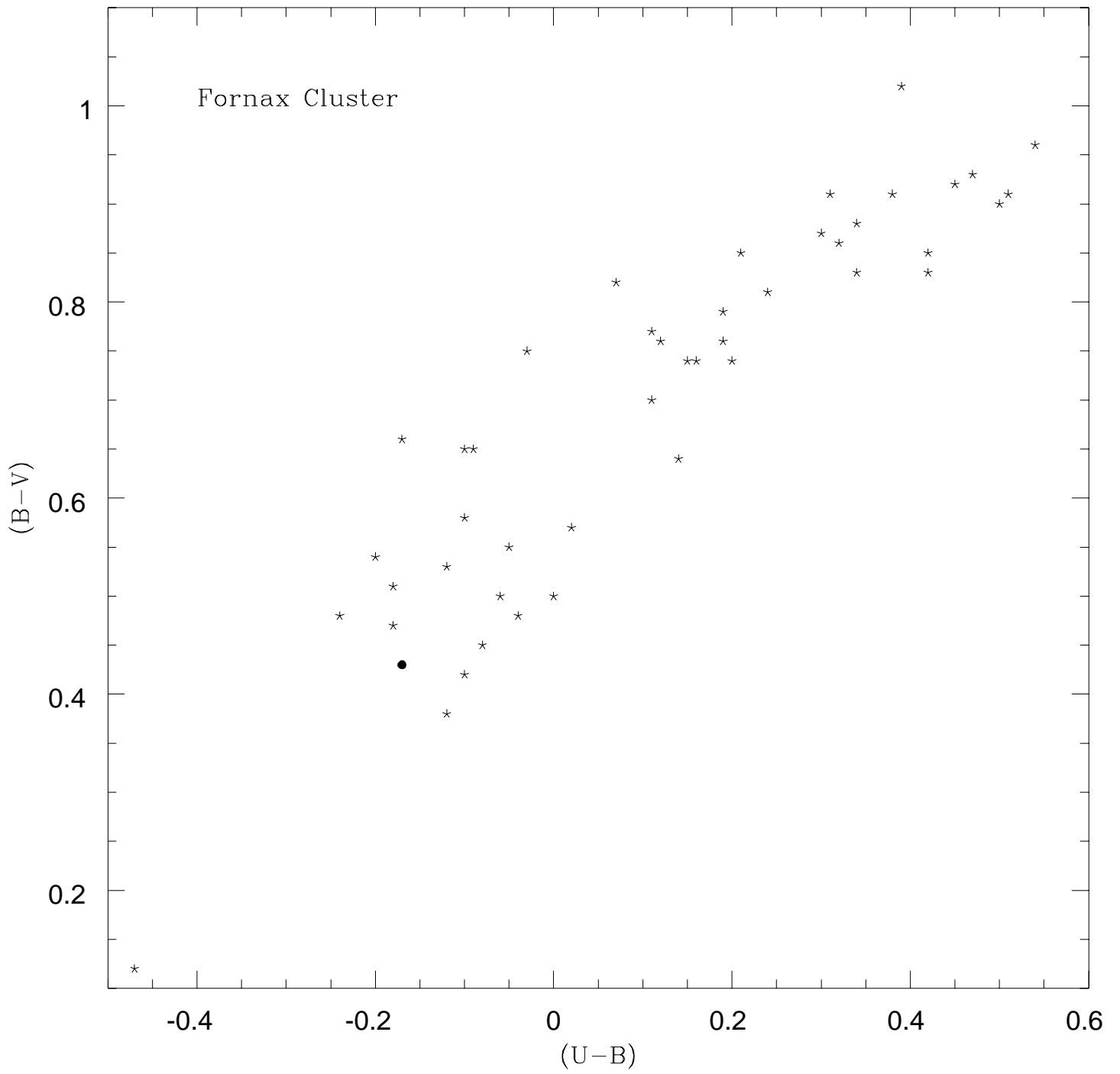
Aperture Radius (")	U	$U - V$
3	17.6	-0.28
4.8	16.8	-0.26
5.7	16.6	-0.25
6.6	16.4	-0.23
9	16.1	-0.18



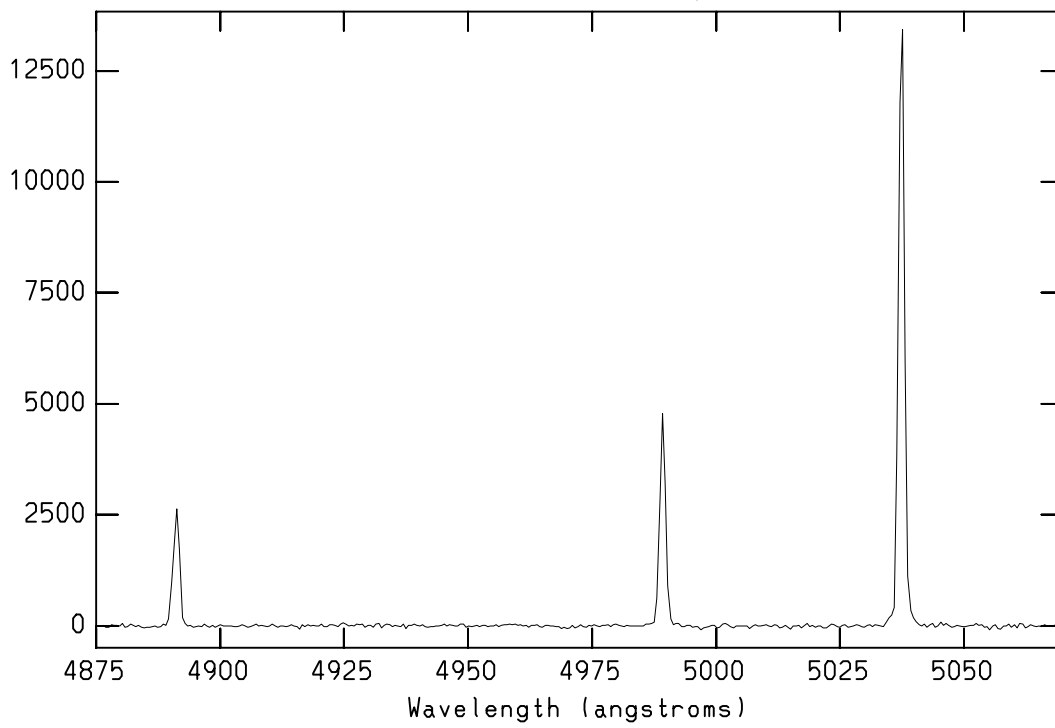








NOAO/IRAF V2.10.4EXPORT putman@mgiant Wed 15:25:04 29-Oct-97
[sum2b]: sum2b.fits INDEF ap:185 beam:0



FCC 35 and its H I Companion: Multi-Wavelength Observations and Interpretation

M.E. Putman¹, M. Bureau¹, J.R. Mould¹, L. Staveley-Smith², and K.C. Freeman¹

¹Mount Stromlo and Siding Spring Observatories, Institute of Advanced Studies, The Australian National University, Private Bag, Weston Creek Post Office, ACT 2611, Australia

²Australia Telescope National Facility, CSIRO, P.O. Box 76, Epping, NSW 2121, Australia

Received _____; accepted _____

ABSTRACT

The Fornax cluster galaxy FCC 35 shows an unusual multiply-peaked integrated H I profile (Bureau, Mould & Staveley-Smith 1996). We have now observed FCC 35 with the Australia Telescope Compact Array (ATCA) and have found a compact H I source with $M_{HI} = 2.2 \times 10^8 M_{\odot}$, and a spatially overlapping complex of H I gas with the same mass. By combining optical observations with the H I data, we are able to identify FCC 35 as a young compact source of star formation with a nearby intergalactic H I cloud which is devoid of stars. We classify FCC 35 as a blue compact dwarf (BCD) or H II galaxy, having large amounts of neutral hydrogen, very blue colors ($(U - V) = 0.1$), and a low metallicity spectrum with strong narrow emission lines. Together with the presence of the H I cloud, this suggests that FCC 35 is the result of a recent interaction within the Fornax cluster.

Subject headings: galaxies: clusters: individual (Fornax) – galaxies: individual (FCC 35) – galaxies: interactions – galaxies: starburst – intergalactic medium – ISM: clouds

1. Introduction

Our interest in FCC 35 began in 1994 when this galaxy was observed as part of an investigation of the Tully-Fisher relation in Fornax (Bureau, Mould, & Staveley-Smith 1996; hereafter BMS). Optically, FCC 35 was identified as a member of the Fornax cluster by Ferguson (1989) and classified as a possible BCD/Sm IV. BMS photometry revealed a high surface brightness and an offset nucleus, despite a regular light profile. The 21 cm single-dish observations of FCC 35 showed three distinct H I peaks within a 700 km s^{-1} velocity range (see Fig. 1). There were no other known H I sources within the Parkes’ beam, so the explanation for the three-peaked profile was unknown. This anomaly served to motivate further studies of FCC 35.

Generally, BCDs like FCC 35 are high surface brightness dwarf galaxies which appear to be undergoing an intense period of star formation (Thuan & Martin 1981). The cause of these star formation bursts is not well understood, but in many cases interaction is considered a likely mechanism. Interactions can induce rapid star formation (Bushouse 1987) and the resulting internal motions can continue to induce bursts for up to 10^8 yrs after the interaction (Noguchi 1991). There are several types of interaction which can trigger the BCD phenomenon. The first involves an encounter between two spiral galaxies and the formation of H I-rich tidal tails. BCDs have been observed and modeled to form at the end of these tails which can extend for hundreds of kpc (e.g. Duc et al. 1997; Barnes & Hernquist 1992, 1996; Elmegreen, Kaufman & Thomasson 1993; Mirabel, Lutz & Maza 1991; Schweizer 1978). The surrounding environment is often left in a disordered state for some time after this type of interaction. Another type of starburst-inducing interaction involves an intergalactic H I cloud of similar mass to the progenitor galaxy (Taylor, Brinks & Skillman 1993, Taylor 1997). Taylor et al. (1995, 1996) completed a survey of relatively isolated BCDs (also called H II galaxies) and found $\approx 57\%$ of these to have an H I companion which could be triggering the star formation burst. Finally, close encounters between two galaxies of different mass often induce star formation in the smaller component, possibly creating a BCD (Ostlin & Bergvall 1993; Lacey & Silk 1991). Putting all of these possibilities together strongly suggests that the star formation bursts which produce BCDs are indeed due to interactions.

In a cluster environment these interactions are much more likely to occur than in the field. The denser the environment, the higher the potential for an interaction among member galaxies. Fornax is a well-studied nearby cluster ($d = 18.2 \text{ Mpc}$; Madore et al. 1996) which has one of the highest galaxy volume densities in the Local Supercluster (Held & Mould 1994) and more than twice the central surface density of Virgo (Ferguson & Sandage 1988). The relatively low velocity dispersion of Fornax ($\approx 400 \text{ km s}^{-1}$) further favors

interaction between cluster members. FCC 35 is therefore in an ideal environment to be affected by the mechanisms described above.

The ATCA observations of FCC 35, presented here, reveal two distinct H I sources; one compact and regular associated with the optical FCC 35, and one extended and irregular with no optical counterpart. The sources overlap spatially but are separated by 140 km s^{-1} in velocity. These observations indicate that FCC 35 has an H I companion of comparable mass. This brings us to the various interaction scenarios. The starburst which is now FCC 35 may be due to a previous interaction with this H I source or both components could be the result of a spiral-spiral interaction. It is also conceivable that the H I companion itself resulted from a gas outflow associated with the star formation burst. Investigating these possibilities is one of the central topics of this paper.

In this paper we present a combination of data which helps to reveal the origin and evolution of FCC 35. We discuss the ATCA observations and data reduction in §2.1 and the optical imaging and spectroscopy in §2.2. In §3.0 we present the results of these observations, including the H I distribution (§3.1), H I kinematics (§3.2), stellar distribution (§3.3), and physical conditions of the gas (§3.4). Finally, in §4.0, we discuss these results and their implications for the formation and evolution of dwarf galaxies, in particular with respect to various interaction scenarios. The 21 cm and optical observations together provide a unique source of information on the nature of BCDs and their companions in clusters.

2. Observations

2.1. Radio Synthesis Observations

21 cm line data were obtained with the ATCA using three configurations and all six antennas. The observing log can be found in Table 1. The total bandwidth of the spectral line data was 8 MHz or 1688 km s^{-1} , encompassing all three of the peaks which were detected in the Parkes observations (see Fig. 1). The central velocity was 1550 km s^{-1} , with 512 channels in each polarization spaced by 3.3 km s^{-1} . Continuum data centered at 1380 MHz was also obtained during the ATCA observations, but FCC 35 remained undetected at the 0.45 mJy level.

The spectral line data were loaded and immediately Hanning smoothed in MIRIAD, resulting in 256 channels at a velocity resolution of 6.6 km s^{-1} . Bad data were flagged interactively by examining both the phase and amplitude for suspect times and baselines. The bandpass and flux level were calibrated using

the primary calibrator PKS B1934-638, which was observed at the beginning of each run. The gain and phase were calibrated using the secondary calibrators listed in Table 1; these were observed every 45 minutes during the observations (flux reference: Walsh 1992).

After calibration, the continuum was subtracted in the uv plane using a second order fit to the line free channels. The phase center of the visibility data was moved to the strong continuum source Fornax A in order to achieve a more accurate continuum subtraction. The uv data for each configuration were then combined and imaged using natural weighting, a cell-size of $15'' \times 15''$, and uv spacings out to 8 $k\lambda$. The final cleaned cube has 128×128 pixels and 140 channels, with a resulting beam FWHM of $60'' \times 40''$. The rms noise per channel is 1.2 mJy/beam. A uniformly weighted cube of the same size was also created using a cellsize of $5'' \times 5''$ and a uv taper of 9 $k\lambda$. The beam FWHM in this case is $30'' \times 25''$ and the rms noise per channel is 2 mJy/beam.

2.2. Optical Observations

V and I band images were obtained at the f/8 focus of the 1.0 m telescope at Siding Spring Observatory (SSO). A U band image was subsequently obtained using the Imager on the SSO 2.3 m telescope. A log of the optical observations can be found in Table 2. The scale of the images is $0''.6 \text{ pixel}^{-1}$ and all observations were done under photometric conditions. The data reduction was completed within the IRAF package using standard procedures for bias subtraction and flatfielding with sky flats.

Long-slit optical spectra were also obtained using the Double Beam Spectrograph (DBS) also on the SSO 2.3 m telescope. The slit was positioned along the major axis of FCC 35 and a slit width of $1''.8$ was used, yielding a two-pixel spectral resolution of 1.1 \AA . The pixel scale in the spatial direction is $0''.9 \text{ pixel}^{-1}$. The data were reduced in the standard manner within IRAF. The data were first bias subtracted and flatfielded, and then wavelength calibrated using bracketing comparison lamp exposures. The data were then rebinned to a linear wavelength scale, slit corrected, and sky and continuum subtracted to “isolate” emission lines. Because the resulting spectra did not show any obvious velocity gradient or variation in line ratios across the galaxy, the data were collapsed spatially over $27''$ to increase the signal-to-noise ratio. After reduction, the wavelength range was 4800 - 5750 \AA in the blue arm spectrum and 6070 - 7020 \AA in the red arm, with a scale of $0.55 \text{ \AA pixel}^{-1}$. Because no spectrophotometric standard was observed, only line ratios of closely spaced lines are meaningful.

3. Results

3.1. H I Distribution

The ATCA cubes do not show emission at 1275 km s^{-1} , a peak which was originally detected in the Parkes observations (see Fig. 1). In the naturally weighted cube (Fig. 2), the first emission appears at approximately 1635 km s^{-1} and continues to 1675 km s^{-1} , covering only 40 km s^{-1} . There is no emission detected between 1675 and 1755 km s^{-1} , and then emission appears again in the same general region as the first source. This emission is stronger and extends from 1760 km s^{-1} to 1840 km s^{-1} . It has a regular structure and is relatively compact. The optical velocity of FCC 35 is about 1814 km s^{-1} (see §3.4) so we identify this peak with FCC 35 itself (this source is also coincident with the optical position of FCC 35 (see Fig. 3)), while classifying the first source as an H I cloud, separated from FCC 35 by 140 km s^{-1} (peak to peak). The H I cloud has an irregular ring-like structure (see Fig. 2) and no optical counterpart (see §3.3). In the uniformly weighted cube, the overall structure of FCC 35 does not change, but the H I cloud is resolved out.

The ATCA fluxes were obtained using the task BLANK in AIPS to select the channels and regions which contained emission. The flux densities for these regions were then summed together and multiplied by the channel spacing. For FCC 35, the ATCA flux is approximately equal to the Parkes' value (see Table 3), resulting in an H I mass of $2.2 \times 10^8 M_{\odot}$ and a maximum H I column density of $1.1 \times 10^{20} \text{ cm}^{-2}$. The ATCA observations of the extended H I cloud are most likely missing flux due to the absence of short spacings. The single-dish observations give an integrated H I flux of 2.9 Jy km s^{-1} for the H I cloud, while the ATCA gives a value of 1.4 Jy km s^{-1} (see Fig. 1; values are listed in Table 4). We adopted the Parkes flux as the most accurate value, giving an H I mass of $2.2 \times 10^8 M_{\odot}$, or equal to FCC 35. The maximum H I column density for the H I cloud using the ATCA data is $2.0 \times 10^{19} \text{ cm}^{-2}$. The 1275 km s^{-1} peak may be an extended H I source which was lost in the ATCA data due to missing uv spacings. Future work should include observations with more compact configurations to attempt to recover this source.

Moment maps were made of both the H I cloud and FCC 35 using the MOMNT task within AIPS and the naturally weighted data cube. The channels ranging from $1761 - 1847 \text{ km s}^{-1}$ were used to create the moment maps of FCC 35, and the channels ranging from $1629 - 1675 \text{ km s}^{-1}$ were used for the H I cloud. Data greater than and equal to 3 mJy/beam ($\approx 3\sigma$) were included in the maps. In Figs. 3 and 4 we show the H I integrated intensity contour maps of FCC 35 and the H I cloud overlaid on an optical image. From these pictures it is apparent that the high velocity source is associated with FCC 35, while the low velocity

source does not appear to have an optical counterpart. The extended nature of the H I is also evident in this figure.

3.2. H I Kinematics

The velocity field of FCC 35 is fairly regular, as shown in Fig. 5. The H I cloud does not have any obvious kinematical structure (Fig. 6). An H I rotation curve was derived for FCC 35 using the tilted ring algorithm ROCUR within AIPS (Begeman 1987) and a first moment map created with the uniformly weighted cube (for increased spatial resolution). The galaxy was modeled as a succession of independent rings, each defined by its central coordinates, systemic velocity, inclination, position angle and rotational velocity. The number of rings used in the analysis was limited by the large size of the beam relative to FCC 35’s angular diameter. We oversampled the curve to include several additional points and kept the central coordinates fixed at the optical center of the galaxy. The systemic velocity was fixed at 1800 km s^{-1} after the first run, and the inclination, position angle and rotational velocity were varied according to ROCUR’s analysis. After several trial runs, the inclination and position angle were fixed at 13° and 62° respectively, and a rotational velocity was obtained for each ring (Fig. 7). The entire galaxy was used in this analysis. Rotation curves were also obtained for the receding and approaching halves of the galaxy separately, but they differed only slightly from Fig. 7.

Fig. 7 suggests that the rotation curve may be turning over at our last data point, with a maximum rotational velocity of $\approx 21 \text{ km s}^{-1}$ at a radius of $54''$. Assuming circular motion, we derive an enclosed mass of $4.8 \times 10^8 M_\odot$ at this radius. This is probably an underestimate, because pressure support is usually significant in BCDs (e.g. Meurer et al. 1996; Hunter et al. 1996, 1994). Indeed, for FCC 35 the ratio of V_{rot}^2 to σ_v^2 in the outer disk indicates that random motions contribute greater than 20% of the support and a cursory examination with the AIPS tasks XGAUS and MOMNT suggest an increase in linewidth towards the center of the galaxy. In light of this, we attempted to account for pressure support by calculating an asymmetric drift correction (Fig. 8).

The asymmetric drift correction was determined with the method described by Meurer et al. (1996), using the radial profile of the H I surface density and velocity dispersion. Our beam size limits the analysis, but adding the correction to our original rotation curve gives a (corrected) circular velocity curve (Fig. 8; Table 5) which peaks at $\approx 40''$ (30 km s^{-1}) and subsequently shows a Keplerian decline. This suggests that the mass distribution of this galaxy may be severely truncated. Fig. 8 shows that the corrected velocity at $60''$

is the same as our uncorrected rotational velocity at this radius, so our mass estimate is unaffected. However, it now represents the total mass of FCC 35 (rather than the mass enclosed within our last measured point). Adopting $4.8 \times 10^8 M_{\odot}$ as the total mass gives an M_{tot}/L_V ratio of approximately $3 M_{\odot}/L_{\odot}$. We have not attempted a detailed mass model at this stage due to the large beamsize. We defer this analysis until higher resolution H I observations are obtained. However, the results at this stage seem clear: a Keplerian decline in the velocity curve, which indicates a truncation of mass, low dark matter content and a low M_{tot}/L_V .

3.3. Optical Photometry

FCC 35's U (Fig. 9a) and V band images reveal an off-center nucleus which is not present in the I band image (Fig. 9b). There is no optical counterpart for the HI cloud (Fig. 4) (any galaxy with a surface brightness of $V = 26 \text{ mag/arcsec}^2$ or $M_V = -14$ would have been detected). The photometric calibration for these images was derived using Graham (1982) and Landolt (1992) standards (see also Bessell 1995) and DAOPHOT in IRAF. Elliptical isophotes were fit to each image using GASP and the remaining data processing was completed within the SFOTO package (Han 1991). The derived magnitudes were corrected for atmospheric and galactic extinction. Elliptical apertures give a $(U - V)_{22''.5} = 0.1$ and $(U - V)_{14''} = 0.0$. The total V band magnitude quoted in Table 3 was obtained by assuming an exponential light profile in the outer parts of the disk. The U band surface brightness profile can be found in Fig. 10, with the V and I band profiles behaving similarly. All of the profiles are tabulated in Table 6. Fig. 10 appears to flatten out at the center of the galaxy, but it may be somewhat ill-determined here due to the off-center nucleus (see Fig. 9a). A separate analysis was carried out on the galaxy's nucleus using circular apertures with the task PHOT in IRAF. This analysis reveals successively bluer colors with decreasing radius (Table 7). As shown in Fig. 11 (Schröder 1995), FCC 35 is one of the bluest galaxies in the Fornax cluster, reflecting its star formation activity.

3.4. Optical Spectrum

FCC 35's spectrum (Fig. 12) shows strong $H\alpha$, [OIII] $\lambda\lambda 4959, 5007$ and $H\beta$ emission. The [NII] $\lambda 6584$ line is marginally detected and [SII] $\lambda\lambda 6716, 6731$ and HeI $\lambda 6678$ are weak but present. The ratio [NII]/ $H\alpha$ has an upper limit of 0.04 and [OIII]/ $H\beta$ has a value of approximately 4.8. Using theoretical photoionization models of extragalactic H II regions (Dopita & Evans 1986; Sutherland & Dopita 1993), we derive an upper

limit on the metallicity of $0.25 Z_{\odot}$, which is normal for the absolute magnitude of FCC 35 (see Table 3). This value is typical for BCDs (e.g. II Zw 40; Walsh & Roy 1993), but nowhere near as low as I Zw 18 (Masegosa, Moles & Campos-Aguilar 1994). The optical emission lines are extremely narrow. The optical heliocentric velocity is $\approx 1814 \text{ km s}^{-1}$, corresponding to the higher velocity H I peak.

4. Discussion

4.1. The H I Cloud

A position-velocity cut through the center of both FCC 35 and the H I cloud (Fig. 13) shows that despite the spatial overlap, the two components are not connected in velocity space. The cloud may either be a unique source within the Fornax cluster or a foreground or background H I object. The former seems to be the most likely considering the velocity of the cloud ($V_{r,\odot} = 1658 \text{ km s}^{-1}$) and the mean heliocentric velocity of the Fornax cluster ($\langle v \rangle = 1450 \pm 34 \text{ km s}^{-1}$, $\sigma_v = 350 \text{ km s}^{-1}$; Held & Mould 1994).

The Fornax cluster has a central number density of $500 \text{ galaxies Mpc}^{-3}$ (Ferguson 1989), and tidal debris from interactions should be expected (e.g. Theuns & Warren 1997). Some of the intergalactic material may be primordial, but in a dense cluster it is likely to have arisen from galactic harassment (Moore et al. 1996). This is especially true when considering the proximity of our H I cloud to the center of the Fornax cluster ($03^h35^m, -35.7^\circ$; Ferguson 1989). The interaction which formed the cloud may not have involved the galaxy FCC 35, and the cloud may simply be “passing by” at this stage. Its structure could be affected by FCC 35’s presence (see Figs. 2 & 4), but this is difficult to confirm due to the irregular kinematics of the cloud and the sensitivity of its inferred structure on the weighting used in the reduction.

It is also possible that the H I cloud is a remnant of an interaction in which FCC 35 was involved. We note that NGC 1316C is located only $6'$ away (in projection) from FCC 35 ($\Delta V = 150 \text{ km s}^{-1}$) and the two could have interacted in the past. It is conceivable that FCC 35 and the cloud were a single object which was ripped apart tidally into two parts of comparable mass. This seems unlikely, however, considering the regular and compact structure of FCC 35.

Yet another possibility is that the H I cloud *and* FCC 35 formed through an interaction between two spirals. Dwarf galaxies and massive H I clouds have been predicted to form (Barnes & Hernquist 1992; Elmegreen et al. 1993) and observed forming (Schweizer 1978; Mirabel et al 1991) in the tidal tails which arise from these interactions. The H I cloud could then be the remaining gas from a tidal tail. This possibility

will be discussed further in the next section.

4.2. FCC 35

The amount of neutral hydrogen in FCC 35 ($M_{HI}/M_{Tot} = 0.5$), together with the optical data, presents a picture of a blue compact dwarf (BCD) or H II galaxy. Exponential surface brightness profiles are typical of BCDs (see Fig. 10), as are offset nuclei (Fig. 9a; Drinkwater & Hardy 1991). The spectrum of FCC 35 is also similar to that of the general BCD population, with relatively low metallicity and strong narrow emission lines (Fig. 12; Izotov et al. 1997; Masegisa et al. 1994; Walsh & Roy 1993; Thuan & Martin 1981). The strong H α and [OIII] emission lines are a signature of the star formation activity in FCC 35, as are the blue colors towards the galaxy’s nucleus (see Table 7).

The formation of BCDs is still not understood. Interaction may be responsible for a significant fraction, but there are also explanations based upon an evolutionary sequence among dwarf galaxies. Davies & Phillipps (1988) propose a sequence, dI \leftrightarrow BCD \leftrightarrow dE, which involves repeatedly induced star formation bursts and explains the similarities between different types of dwarf galaxies. The trigger of the BCD phenomenon is described by Gordon & Gottesman (1981). They find the majority of dwarf irregulars to have an extended H I halo and suggest that the infall of this halo fuels the star formation bursts. FCC 35 does have an extended H I halo, but the presence of the H I cloud suggests that this star formation burst is interaction related.

One type of interaction which has been found to produce BCDs and intergalactic H I clouds is the interaction between two spiral galaxies. The tidal tails formed as a result of these interactions can extend for hundreds of kpc (Hibbard & Van Gorkom 1996) and create objects of up to $10^9 M_{\odot}$ (Elmegreen et al. 1993). The tidal features often have low mass-to-light ratios (Hibbard & Van Gorkom 1996), and the models of Barnes and Hernquist (1992) predict that these objects would have very little dark matter. Elmegreen et al. (1993) also predict that dwarf galaxies formed as a result of this type of interaction should contain old stars from the original disks plus new stars from the interaction-induced star formation bursts. FCC 35’s upper limit on the ionized gas abundance ($Z \leq 0.25 Z_{\odot}$) is consistent with tidal formation from the outer disk of a spiral galaxy. Indeed, FCC 35 fulfills many of the criteria related to the spiral-spiral interaction scenario (see Table 3). It has a relatively low M_{tot}/L_V and a (corrected) rotation curve (Fig. 8) which indicates a truncated mass distribution and (presumably) small amounts of dark matter. However, if this is the origin of FCC 35, we would perhaps expect to observe more remnant H I in the surrounding region. This was not

apparent in the channel maps obtained within the $43'$ primary beam of the ATCA.

FCC 35's star formation burst could also have been induced through an interaction with its closest neighbor, NGC 1316C, which has not been detected in H I. However, this scenario appears unlikely when the age of FCC 35's star burst is taken into account. Its color, $(U-V)_{26''} = 0.1$, corresponds to an age of about 10^7 years (Larson & Tinsley 1978). If FCC 35's star formation burst had been directly triggered by an interaction with NGC 1316C, the relative speed of NGC 1316C would need to be at least 3000 km s^{-1} . This is excessive given the low velocity dispersion of the Fornax cluster. However, we recall that internal motions resulting from interactions can induce later star formation bursts (Noguchi 1991), so our arguments do not conclusively exclude this possibility or the spiral-spiral interaction scenario.

The most plausible interaction-related cause for the star formation burst in FCC 35 is that the H I cloud, whatever its origin, has triggered it. Its relative mass and its proximity in space and velocity make it likely that the cloud is interacting with FCC 35. This situation is not uncommon: Taylor et al. (1994) find that galaxies with H I companions tend to have a very low mass-to-light ratios and the mass of the companion is often only an order of magnitude smaller than the mass of the galaxy (see also Walter et al. 1997). The relative velocity, projected separation, and masses of the H I cloud and FCC 35 clearly show that they are unbound, so it seems likely that they will drift apart as FCC 35 fades into a low surface brightness or irregular dwarf galaxy.

5. Summary

We have obtained radio synthesis data, complemented by optical imaging and spectroscopy, of FCC 35, a Fornax member galaxy which has an unusual single-dish H I profile. We discovered a rotationally supported H I disk associated with FCC 35 and an irregularly shaped H I cloud. FCC 35 and the H I cloud have approximately equal H I masses and the two sources overlap spatially yet are completely separate in velocity. The cloud has no kinematical structure, while FCC 35 has a rotation curve which indicates a truncated mass distribution. U and V band images depict an offset nucleus in FCC 35 and no optical counterpart for the H I cloud. FCC 35 has very blue $U - V$ colors and strong H_α and [OIII] emission lines, indicating it is a source of active star formation. The data indicate that the H I cloud is most likely triggering the star formation burst in FCC 35. Whatever FCC 35's origin and fate, it is an interesting source of information on the evolution of dwarf galaxies in a cluster environment. Further work should investigate FCC 35's surrounding environment and explore its possible influence on the gas which has become FCC 35.

Deep H I searches for intergalactic clouds in clusters should be pursued in Fornax as well as other clusters.

MEP and MB acknowledge the support of an Australian DEETYA Overseas Postgraduate Research Scholarship. MB also acknowledges the support of a Canadian NSRC Postgraduate Scholarship. We thank the staff of Mount Stromlo and Siding Spring Observatories and of the Australia Telescope National Facility for their assistance during and after the observations. In particular, Richard Gooch for his help in maintaining the Karma Visualization Software, Helmut Jerjen for his help with the observations and Mike Dopita for the use of the MAPPINGS program. We also thank the anonymous referee for useful comments. The Australia Telescope is funded by the Commonwealth of Australia for operation as a National Facility managed by CSIRO. The Digitized Sky Surveys were produced at the Space Telescope Science Institute under U.S. Government grant NAG W-2166. The images of these surveys are based on photographic data obtained using the Oschin Schmidt Telescope on Palomar Mountain and the UK Schmidt Telescope. The plates were processed into the present compressed digital form with the permission of these institutions.

REFERENCES

- Barnes, J. E., & Hernquist, L. 1996, *ApJ*, 471, 115
- Barnes, J. E., & Hernquist, L. 1992, *Nature*, 360, 715
- Begeman, K. 1987, Ph.D. Thesis, University of Groningen
- Bessell, M. S. 1995, *PASP*, 107, 672
- Bureau, M., Mould, J. R., & Staveley-Smith, L. 1996, *ApJ*, 463, 60
- Bushouse, H. A. 1987, 320, 49
- Davies, J. I., & Phillipps, S. 1988, *MNRAS*, 233, 553
- Dopita, M. A. & Evans, I. N. 1986, *ApJ*, 307, 431
- Drinkwater, M., & Hardy, E. 1991, *AJ*, 101, 94
- Duc, P. A., Brinks, E., Wink, J. E. & Mirabel, I. F. 1997, *A&A*, 326, 537
- Elmegreen, B. G., Kaufmann, M., & Thomasson, M. 1993, *ApJ*, 412, 90
- Ferguson, H. C. 1989, *AJ*, 98, 367
- Ferguson, H. C. & Sandage, A. 1988, *AJ*, 96, 1520
- Gordon, D., & Gottesman, S. T. 1981, *AJ*, 86, 161
- Graham, J. A. 1982, *PASP*, 94, 244
- Han, M. S. 1991, Ph.D. Thesis, California Institute of Technology
- Held, E. V., & Mould, J. R. 1994, *AJ*, 107, 1307
- Hibbard, J. E., & Van Gorkom, J. H. 1996, *AJ*, 111, 655
- Hunter, D. A., Van Woerden, H., & Gallagher, J. S. 1996, *ApJS*, 107, 739
- Hunter, D. A., Van Woerden, H., & Gallagher, J. S. 1994, *ApJS*, 91, 79
- Izotov, Y. I., Lipovetsky, V. A., Chaffee, F. H., Foltz, C. B., Guseva, N. G., & Kniazev, A. Y. 1997, *ApJ*, 476, 698
- Lacey, C., & Silk, J. 1991, *ApJ*, 381, 14
- Landolt, A. U. 1992, *AJ*, 104, 340

- Larson, R. B., & Tinsley, B. M. 1978, ApJ, 219, 46
- Madore, B. F. et al 1996, BAAS, 189, 108.04
- Masegosa, J., Moles, M., & Campos-Aguilar, A. 1994, ApJ, 420, 576
- Meurer, G. R., Carignan, C., Beaulieu, S. F., & Freeman, K. C. 1996, AJ, 111, 1551
- Meurer, G. R., Mackie, G., & Carignan, C. 1994, AJ, 107, 2021
- Mirabel, I. F., Lutz, D., & Maza, J. 1991, A&A, 243, 367
- Moore, B., Katz, N., Lake, G., Dressler, A., & Oemler, Jr., A. 1996, Nature, 379, 613
- Noguchi, M. 1991, MNRAS, 251, 360
- Ostlin, G., & Bergvall, N. 1993, in ESO Conference and Workshop Proceedings No. 49, ed. G. Meylan & P. Prugniel, 451
- Schröder, A. 1995, Ph.D. Thesis, University of Basel
- Schweizer, F. 1978, in Structure and Properties of Nearby Galaxies, ed. E. M. Berkhuijsen & R. Wielebinski (Dordrecht: Reidel), 279
- Sutherland, R. S., & Dopita, M. A. 1993, ApJS, 88, 253
- Taylor, C. L. 1997, ApJ, 480, 524
- Taylor, C. L., Brinks, E., Grashuis, R. M., & Skillman, E. D. 1996, ApJS, 102, 189
- Taylor, C. L., Brinks, E., Grashuis, R. M., & Skillman, E. D. 1995, ApJS, 99, 427
- Taylor, C. L., Brinks, E., Pogge, R. W., & Skillman, E. D. 1994, AJ, 107, 971
- Taylor, C. L., Brinks, E., & Skillman, E. D. 1993, AJ, 105, 128
- Thuan, T. X., & Martin, G. E. 1981, ApJ, 247, 823
- Theuns, T., & Warren, S. J. 1997, MNRAS, 284, L11
- Walsh, W., editor 1992, Australia Telescope Compact Array Users Guide (Version 1.0), (Australia Telescope National Facility, Sydney)
- Walsh, J.R., & Roy, J.-R. 1993, MNRAS, 262, 27
- Walter, F., Brinks, E., Duric, N., & Klein, U. 1997, AJ, 113, 2031

Fig. 1.— FCC 35's 21 cm line profile as measured with the Parkes Telescope (bold line) and the ATCA (thin line). The Parkes spectrum has been corrected for the offset used in the observations (a correction factor of 1.38).

Fig. 2.— Naturally weighted channel maps for the 21 cm ATCA data. The heliocentric velocity is shown in the upper left corner of each channel and the cross marks the optical center of FCC 35. The beam is shown in the lower left corner of the first channel. Contours range from 5 - 40 mJy/beam in steps of 6 mJy/beam, with an rms per channel of 1.2 mJy/beam.

Fig. 3.— DSS image overlaid on the H I integrated intensity contours of FCC 35. The image is $10' \times 10'$ and the contours range from 3 - 170 mJy/beam in steps of 16 mJy/beam. The beam is shown in the lower left corner.

Fig. 4.— DSS image overlaid on the H I integrated intensity contours of the H I cloud. The image is $10' \times 10'$ and the contours range from 3 - 34.5 mJy/beam in steps of 4.5 mJy/beam. The beam is shown in the lower left corner.

Fig. 5.— Velocity contours of FCC 35. Several of the contours are labeled in km s^{-1} .

Fig. 6.— Velocity contours of the H I cloud. The contours have no obvious gradient and are labeled in km s^{-1} .

Fig. 7.— Uncorrected rotation curve of FCC 35 using both sides of the galaxy.

Fig. 8.— Corrected rotation curve of FCC 35 (solid circles). The open circles show the H I rotation curve from Fig. 7, and the solid line represents the asymmetric drift correction. The data are tabulated in Table 5.

Fig. 9.— a) U band, and b) I band images of FCC 35. Each image is $40'' \times 45''$.

Fig. 10.— U band surface brightness profile of FCC 35. The data for the U, V and I band surface brightness profiles are tabulated in Table 6.

Fig. 11.— Distribution of integrated galaxy colors within the Fornax cluster. FCC 35 is marked as a solid circle. (See Schröder 1995 for more information on the photometry.)

Fig. 12.— a) Blue spectrum of FCC 35, showing H_β and [OIII] $\lambda\lambda$ 4959, 5007. b) Red spectrum of FCC 35 showing H_α , [NII] λ 6584, HeI λ 6678, and [SII] $\lambda\lambda$ 6716, 6731. No other lines are seen in the spectra.

Fig. 13.— Position-velocity slice through the centers of both FCC 35 and the H I cloud ($PA=91^\circ$, naturally weighted cube).

Table 1. H I Observing Log

UT date	Configuration name	Baseline range (m)	On source time (hrs)	Secondary calibrators
1997 Mar, 5	6.0A	337 - 5939	5.0	0438-436
1996 May, 17	0.75D	31 - 4469	10.75	0201-440, 0438-436
1996 May, 11	1.5D	107 - 4439	9.75	0201-440, 0438-436

Table 2. Optical Observing Log

UT Date	Data	Telescope	Instrument	CCD (pixels)	Exposure Time (sec)
1997 Mar, 12	Spectra	SSO 2.3m	DBS	1752 × 532 SITE	2000
1997 Mar, 11	U image	SSO 2.3m	Imager	1024 × 1024 SITE	1200
1994 Dec, 12	V image	SSO 1.0m	Direct Imaging	2186 × 1152 EEV	600
1994 Oct, 10	I image	SSO 1.0m	Direct Imaging	2186 × 1152 EEV	900

NOAO/IRAF V2.10.4EXPORT putman@mgiant Wed 15:15:41 29-Oct-97
[sum2r]: sum2r.fits INDEF ap:175 beam:0

